Eur. Phys. J. D **48**, 301–311 (2008)
DOI: 10.1140/epjd/e2008-00108-1

THE EUROPEAN PHYSICAL JOURNAL D

Detuning effects in the vertical cold-atom micromaser

J. Martin[1,a] and T. Bastin[2,b]

[1] Laboratoire de Physique Théorique, Université de Toulouse III, CNRS, 31062 Toulouse, France
[2] Institut de Physique Nucléaire, Atomique et de Spectroscopie, Université de Liège, Bât. B15, 4000 Liège, Belgium

Received 25 March 2008 / Received in final form 9 May 2008
Published online 6 June 2008 –

Abstract. The quantum theory of the cold atom micromaser including the effects of gravity is established in the general case where the cavity mode and the atomic transition frequencies are detuned. We show that atoms which classically would not reach the interaction region are able to emit a photon inside the cavity. The system turns out to be extremely sensitive to the detuning and in particular to its sign. A method to solve the equations of motion for non resonant atom-field interaction and arbitrary cavity modes is presented.

PACS. 42.50.-p Quantum optics – 42.50.Pq Cavity quantum electrodynamics; micromasers – 37.10.Vz Mechanical effects of light on atoms, molecules, and ions

1 Introduction

The coupling of atomic motion to light is a topic of major interest in quantum optics. The mechanical effects of (laser) light on atoms can be exploited to cool, trap and handle the atoms with a great accuracy [1] (see for example [2] for manipulation of individual atoms with optical tweezers). The achieved control on the atomic motion gives rise to a host of applications, like the development of new optical frequency standards based on single ions [3], the realization of an atom laser [4], the possibility of implementing electronic components with atoms (instead of electrons) [5–7], or quantum information processing with cold atoms and trapped ions [8]. In the last example, the interplay between external (motional) and internal degrees of freedom plays a prominent role. This is also the case in the usual micromaser (see Fig. 1) when cold atoms rather than thermal ones are sent through the cavity. Indeed, in this regime a new type of induced emission has been shown to occur because the wave behavior of the atoms becomes important [9]. The resulting process called microwave amplification via z-motion-induced emission of radiation (*mazer*) [9] has opened up a new chapter of micromaser physics [10–19]. In all these papers, gravity effects on the quantized atomic motion are not considered. However, it has often been argued that the achievement of the cold atom micromaser would be a formidable experimental task as the atoms in this regime move so slowly that they start exactly to be extremely sensitive to earth gravity and are expected to fall down before entering or leaving the cavity region, breaking the unidirectionality of the atomic trajectories [20]. A possible way to deal with gravity for the mazer action while keeping the atomic trajectories one-dimensional is to consider a vertical geometry where the atoms are sent vertically in the direction of the cavity, similarly to cavity QED experiments reported in [21–28]. Recently, we established the quantum theory of such a vertical mazer, taking into account gravity effects on the vertical quantized atomic motion [29]. The theory was written for two-level atoms in the resonant case where the cavity mode frequency ω is equal to the atomic transition frequency ω_0. Here, we remove this restriction and investigate the effects of a detuning on the quantum evolution of the combined atom-cavity system in a vertical configuration where gravity action is taken into account.

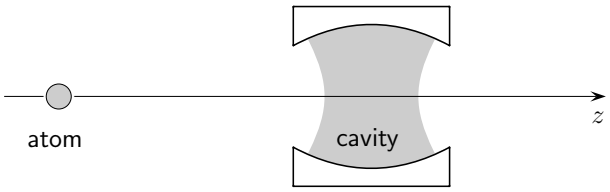

Fig. 1. Scheme of the horizontal micromaser.

The paper is organized as follows. In Section 2, the Hamiltonian modeling our system is presented. The properties of the induced emission probability of a photon inside the cavity are then presented in Section 3. The connection with the classical regime is discussed. A brief summary of our results is finally given in Section 4. In Appendix A, a technical derivation of a specific formula used in our paper is derived. The method we have developed

[a] e-mail: jmartin@irsamc.ups-tlse.fr
[b] e-mail: T.Bastin@ulg.ac.be

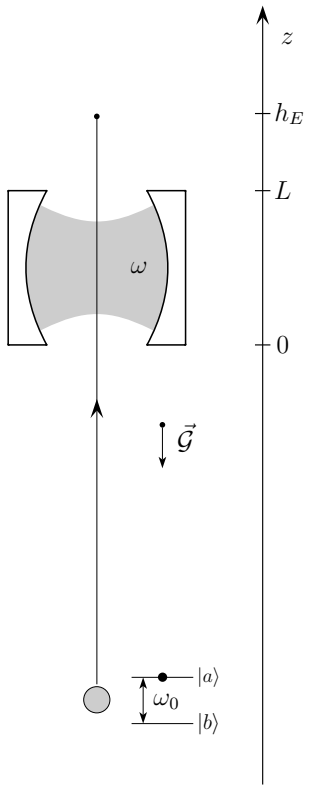

Fig. 2. Scheme of the vertical mazer.

to solve numerically the equations of motion of the mazer in the non resonant case for any mode function is given in Appendix B.

2 Model

2.1 The Hamiltonian

We consider a two-level atom moving in the gravity field along the vertical z direction on the way to a cavity which we define to be located in the range $0 < z < L$ (see Fig. 2). No transverse motion is considered. The atom is coupled nonresonantly to a single mode of the quantized field present in the cavity. The atomic center-of-mass motion is described quantum mechanically and the usual rotating-wave approximation is made. The Hamiltonian thus reads

$$H = \hbar\omega_0\sigma^\dagger\sigma + \hbar\omega a^\dagger a + \frac{p^2}{2m} + m\mathcal{G}z + \hbar g\, u(z)(a^\dagger\sigma + a\sigma^\dagger), \tag{1}$$

where p is the atomic center-of-mass momentum along the z-axis, m is the atomic mass, $\mathcal{G}$ is the acceleration due to gravity, ω_0 is the atomic transition frequency, ω is the cavity field mode frequency, $\sigma = |b\rangle\langle a|$ ($|a\rangle$ and $|b\rangle$ are, respectively, the upper and lower levels of the two-level atom), a and $a^\dagger$ are, respectively, the annihilation and creation operators of the cavity radiation field, g is the atom-field coupling strength, and $u(z)$ the cavity field mode function. We denote in the following the detuning $\omega - \omega_0$ by δ, the cavity field eigenstates by $|n\rangle$, the global state of the atom-field system at any time t by $|\psi(t)\rangle$, and the classical height attained by an atom of energy E in the gravity field by

$$h_E \equiv \frac{E}{m\mathcal{G}}. \tag{2}$$

2.2 The wave functions

We introduce the orthonormal basis

$$\begin{aligned} |\Gamma_n^+(\theta)\rangle &= \cos\theta\,|a,n\rangle + \sin\theta\,|b,n+1\rangle, \\ |\Gamma_n^-(\theta)\rangle &= -\sin\theta\,|a,n\rangle + \cos\theta\,|b,n+1\rangle, \end{aligned} \tag{3}$$

with θ an arbitrary parameter. The $|\Gamma_n^\pm(\theta)\rangle$ states coincide with the noncoupled states $|a,n\rangle$ and $|b,n+1\rangle$ when $\theta = 0$ and with the dressed states when $\theta = \theta_n$ given by

$$\cot 2\theta_n = -\frac{\delta}{\Omega_n}, \tag{4}$$

with the Rabi frequency

$$\Omega_n = 2g\sqrt{n+1}. \tag{5}$$

We denote as $|\pm,n\rangle$ the dressed states $|\Gamma_n^\pm(\theta_n)\rangle$. The Schrödinger equation reads in the z representation and in the basis (3)

$$\begin{aligned} i\hbar\frac{\partial}{\partial t}\psi_{n,\theta}^+(z,t) \;=\; & \Big[-\frac{\hbar^2}{2m}\frac{\partial^2}{\partial z^2} + m\mathcal{G}z + (n+1)\hbar\omega \\ & - \cos^2\theta\,\hbar\delta + \hbar g\,u(z)\sqrt{n+1}\,\sin 2\theta\Big]\psi_{n,\theta}^+(z,t) \\ & + \Big[\hbar g u(z)\sqrt{n+1}\,\cos 2\theta + \frac{\sin 2\theta}{2}\,\hbar\delta\Big]\psi_{n,\theta}^-(z,t), \end{aligned} \tag{6a}$$

$$\begin{aligned} i\hbar\frac{\partial}{\partial t}\psi_{n,\theta}^-(z,t) \;=\; & \Big[-\frac{\hbar^2}{2m}\frac{\partial^2}{\partial z^2} + m\mathcal{G}z + (n+1)\hbar\omega \\ & - \sin^2\theta\,\hbar\delta - \hbar g u(z)\sqrt{n+1}\,\sin 2\theta\Big]\psi_{n,\theta}^-(z,t) \\ & + \Big[\hbar g u(z)\sqrt{n+1}\,\cos 2\theta + \frac{\sin 2\theta}{2}\,\hbar\delta\Big]\psi_{n,\theta}^+(z,t), \end{aligned} \tag{6b}$$

with

$$\psi_{n,\theta}^\pm(z,t) = \langle z, \Gamma_n^\pm(\theta)|\psi(t)\rangle. \tag{7}$$

We get for each n two coupled partial differential equations. In the resonant case ($\delta = 0$), these equations may be decoupled over the entire z-axis when working in the dressed state basis and the atom-field interaction reduces to an elementary scattering problem in the presence of the gravitational field over a potential barrier and a potential well defined by the cavity [29]. In the presence of a detuning, this is no longer the case: there is no basis where equations (6) would separate over the entire z-axis and the interpretation of the atomic interaction with the cavity as a scattering problem over two potentials is less

obvious as it is also the case when gravity is not taken into account [16].

In the noncoupled state basis ($\theta = 0$), equations (6) read

$$i\hbar\frac{\partial}{\partial t}\psi_n^a(z,t) = \left[-\frac{\hbar^2}{2m}\frac{\partial^2}{\partial z^2} + m\mathcal{G}z\right]\psi_n^a(z,t) + \hbar g u(z)\sqrt{n+1}\,\psi_{n+1}^b(z,t), \tag{8a}$$

$$i\hbar\frac{\partial}{\partial t}\psi_{n+1}^b(z,t) = \left[-\frac{\hbar^2}{2m}\frac{\partial^2}{\partial z^2} + m\mathcal{G}z + \hbar\delta\right]\psi_{n+1}^b(z,t) + \hbar g u(z)\sqrt{n+1}\,\psi_n^a(z,t), \tag{8b}$$

with

$$\psi_n^a(z,t) = e^{i(\omega_0+n\omega)t}\,\langle z,a,n|\psi(t)\rangle, \tag{9a}$$

$$\psi_{n+1}^b(z,t) = e^{i(\omega_0+n\omega)t}\,\langle z,b,n+1|\psi(t)\rangle. \tag{9b}$$

In equations (9), we have introduced the exponential factor $e^{i(\omega_0+n\omega)t}$ in order to define the energy scale origin at the $|a,n\rangle$ level. If we assume initially a monoenergetic excited atom coming upwards upon the cavity that contains n photons, the atom-field system is described outside the cavity by the wave function components (which correspond to the eigenstate $|\phi_E\rangle$ of energy E)

$$\psi_n^a(z,t) = e^{-iEt/\hbar}\,\varphi_{E,n}^a(z), \tag{10a}$$

$$\psi_{n+1}^b(z,t) = e^{-iEt/\hbar}\,\varphi_{E,n+1}^b(z), \tag{10b}$$

with $\varphi_{E,n}^a(z)$ and $\varphi_{E,n+1}^b(z)$ obeying

$$\left(-\frac{\hbar^2}{2m}\frac{\mathrm{d}^2}{\mathrm{d}z^2} + m\mathcal{G}z - E\right)\varphi_{E,n}^a(z) = -\hbar g u(z)\sqrt{n+1}\,\varphi_{E,n+1}^b(z), \tag{11a}$$

$$\left(-\frac{\hbar^2}{2m}\frac{\mathrm{d}^2}{\mathrm{d}z^2} + m\mathcal{G}z - E + \hbar\delta\right)\varphi_{E,n+1}^b(z) = -\hbar g u(z)\sqrt{n+1}\,\varphi_{E,n}^a(z). \tag{11b}$$

Introducing, for any length x, the dimensionless variable

$$\tilde{x} \equiv x/\ell \tag{12}$$

with

$$\ell = \left(\frac{2m^2\mathcal{G}}{\hbar^2}\right)^{-1/3}, \tag{13}$$

equations (11) read

$$\left(\frac{\mathrm{d}^2}{\mathrm{d}\tilde{z}^2} - \tilde{z} + \tilde{h}_E\right)\varphi_{E,n}^a(\tilde{z}) = \tilde{h}_{\mathrm{int}}\,u(\tilde{z})\,\varphi_{E,n+1}^b(\tilde{z}), \tag{14a}$$

$$\left(\frac{\mathrm{d}^2}{\mathrm{d}\tilde{z}^2} - \tilde{z} + \tilde{h}_E - \tilde{\delta}\right)\varphi_{E,n+1}^b(\tilde{z}) = \tilde{h}_{\mathrm{int}}\,u(\tilde{z})\,\varphi_{E,n}^a(\tilde{z}), \tag{14b}$$

where

$$\tilde{h}_{\mathrm{int}} = \tilde{g}\sqrt{n+1}, \tag{15}$$

and

$$\tilde{g} = \frac{\hbar g}{m\mathcal{G}\ell}, \quad \tilde{\delta} = \frac{\hbar\delta}{m\mathcal{G}\ell}. \tag{16}$$

The characteristic length ℓ (Eq. (13)) gives the spatial scale of the oscillations of the wave function of a particle in the gravitational field near its turning point. For rubidium atoms, $\ell \simeq 0.3\,\mu$m and, roughly, the dimensionless variable $\tilde{\delta}$ is numerically equal to the detuning $\delta/2\pi$ expressed in kHz. Similarly $\tilde{h}_E$ and $\tilde{L}$ yield the classical height h_E and the cavity length L, respectively, in thirds of μm [29].

Outside the cavity, the mode function $u(z)$ vanishes and equations (14) read

$$\left(\frac{\mathrm{d}^2}{\mathrm{d}\tilde{z}^2} - \tilde{z} + \tilde{h}_E\right)\varphi_{E,n}^a(\tilde{z}) = 0, \tag{17a}$$

$$\left(\frac{\mathrm{d}^2}{\mathrm{d}\tilde{z}^2} - \tilde{z} + \tilde{h}_E - \tilde{\delta}\right)\varphi_{E,n+1}^b(\tilde{z}) = 0. \tag{17b}$$

The solutions to equations (17) are given by linear combinations of Airy Ai and Bi functions [30] and may be written in the form

$$\varphi_{E,n}^a(z) = \begin{cases} a_{E,n}^a\,\mathrm{Ai}(\tilde{z} - \tilde{h}_E) & z > L \\ \mathrm{U}(\tilde{z} - \tilde{h}_E) + d_{E,n}^a\,\mathrm{D}(\tilde{z} - \tilde{h}_E) & z < 0 \end{cases} \tag{18}$$

$$\varphi_{E,n+1}^b(z) = \begin{cases} a_{E,n+1}^b\,\mathrm{Ai}(\tilde{z} - \tilde{h}_E + \tilde{\delta}) & z > L \\ d_{E,n+1}^b\,\mathrm{D}(\tilde{z} - \tilde{h}_E + \tilde{\delta}) & z < 0 \end{cases} \tag{19}$$

with

$$\mathrm{U}(\tilde{z}) = \mathrm{Ai}(\tilde{z}) + i\,\mathrm{Bi}(\tilde{z}) \tag{20a}$$

$$\mathrm{D}(\tilde{z}) = \mathrm{Ai}(\tilde{z}) - i\,\mathrm{Bi}(\tilde{z}) \tag{20b}$$

Equations (18) and (19) underline that the wave functions below the cavity consist of an upward and a downward wave (U and D, respectively). Indeed, the probability current densities associated to these two waves are respectively given by

$$j = \pm\frac{\hbar}{\pi m\ell}. \tag{21}$$

For large negative $\tilde{z} - \tilde{h}_E$ values, these two waves behave similarly to plane waves with a z dependent wave vector [29].

Consequently, the following interpretation must be given to solutions (10). The excited atom coming upwards upon the cavity will be found propagating downwards in the upper state or in the lower state with amplitude $d_{E,n}^a$ and $d_{E,n+1}^b$, respectively. However, in contrast to the resonant case, the atom propagating downwards in the lower state $|b\rangle$ possesses a total external energy $E - \hbar\delta$ different from its initial value E. The atomic transition $|a\rangle \to |b\rangle$ induced by the cavity is responsible for a change of the total external atomic energy. According to the sign of the detuning, the cavity will either provide energy to the atom (for $\delta < 0$) or remove energy from the atom (for $\delta > 0$).

This results merely from energy conservation. When, after leaving the cavity region, the atom is passed from the excited state $|a\rangle$ to the lower state $|b\rangle$, the photon number has increased by one unit in the cavity and the internal energy of the atom-field system has varied by the quantity $\hbar\omega - \hbar\omega_0 = \hbar\delta$. This variation needs to be exactly counterbalanced by the external energy of the system, i.e., the total external atomic energy.

Inside the cavity, the problem is much more complex since we have two coupled partial differential equations. In the special case of the mesa mode function ($u(z) = 1$ inside the cavity, 0 elsewhere), the problem is, however, greatly simplified. In the dressed state basis ($\theta = \theta_n$), the Schrödinger equations (6) take the following form inside the cavity:

$$i\hbar\frac{\partial}{\partial t}\psi_n^{\pm}(z,t) = \left[-\frac{\hbar^2}{2m}\frac{\partial^2}{\partial z^2} + m\mathcal{G}z + V_n^{\pm}\right]\psi_n^{\pm}(z,t) \quad (22)$$

with

$$\psi_n^{\pm}(z,t) = e^{i(\omega_0+n\omega)t}\langle z,\pm,n|\psi(t)\rangle \quad (23)$$

and

$$V_n^{+} = \sin^2\theta_n\,\hbar\delta + \hbar g\sqrt{n+1}\,\sin 2\theta_n, \quad (24a)$$
$$V_n^{-} = \hbar\delta - V_n^{+}. \quad (24b)$$

Using equation (4), we have the well-known relations [31]

$$\sin\theta_n = \frac{\sqrt{\Omega_n'+\delta}}{\sqrt{2\Omega_n'}}, \quad \tan\theta_n = \sqrt{\frac{\Omega_n'+\delta}{\Omega_n'-\delta}},$$
$$\cos\theta_n = \frac{\sqrt{\Omega_n'-\delta}}{\sqrt{2\Omega_n'}}, \quad \cot\theta_n = \sqrt{\frac{\Omega_n'-\delta}{\Omega_n'+\delta}}, \quad (25)$$

with the generalized Rabi frequency

$$\Omega_n' = \sqrt{\Omega_n^2+\delta^2}. \quad (26)$$

We thus have

$$V_n^{+} = \hbar g\sqrt{n+1}\,\tan\theta_n, \quad (27a)$$
$$V_n^{-} = -\hbar g\sqrt{n+1}\,\cot\theta_n. \quad (27b)$$

The exponential factor $e^{i(\omega_0+n\omega)t}$ has been introduced as well in equation (23) in order to define the same energy scale inside and outside the cavity. The positive internal energy V_n^{+} increases with positive detunings and vice versa with negative ones. For large positive (resp. negative) detunings, V_n^{+} tends to the $|b,n+1\rangle$ (resp. $|a,n\rangle$) state energy.

The most general solution of equation (22) is given by

$$\psi_n^{\pm}(z,t) = e^{-iEt/\hbar}\,\varphi_{E,n}^{\pm}(z) \quad (28)$$

with

$$\varphi_{E,n}^{\pm}(z) = A_n^{\pm}\,\mathrm{Ai}(\tilde{z}-\tilde{h}_E+\tilde{h}_n^{\pm}) + B_n^{\pm}\,\mathrm{Bi}(\tilde{z}-\tilde{h}_E+\tilde{h}_n^{\pm}), \quad (29)$$

where $A_n^{\pm}$ et $B_n^{\pm}$ are complex coefficients and $h_n^{\pm} = V_n^{\pm}/m\mathcal{G}$, i.e.

$$h_n^{+} = h_{\mathrm{int}}\tan\theta_n, \quad (30a)$$
$$h_n^{-} = -h_{\mathrm{int}}\cot\theta_n. \quad (30b)$$

From equation (3), we may express the wave function components of the atom-field state inside the cavity over the non-coupled state basis. We have

$$\psi_n^{a}(z,t) = \cos\theta_n\psi_n^{+}(z,t) - \sin\theta_n\psi_n^{-}(z,t), \quad (31a)$$
$$\psi_{n+1}^{b}(z,t) = \sin\theta_n\psi_n^{+}(z,t) + \cos\theta_n\psi_n^{-}(z,t). \quad (31b)$$

This allows us to find the wave function components of the eigenstate $|\phi_E\rangle$ over the entire z-axis. The relations (10) hold with

$$\varphi_{E,n}^{a}(z) = \begin{cases} a_{E,n}^{a}\,\mathrm{Ai}(\tilde{z}-\tilde{h}_E) & z > L, \\ \varphi_{E,n}^{a}(z)\big|_{\mathrm{c}} & 0 \leqslant z \leqslant L, \\ \mathrm{U}(\tilde{z}-\tilde{h}_E) + d_{E,n}^{a}\,\mathrm{D}(\tilde{z}-\tilde{h}_E) & z < 0, \end{cases} \quad (32)$$

$$\varphi_{E,n+1}^{b}(z) = \begin{cases} a_{E,n+1}^{b}\,\mathrm{Ai}(\tilde{z}-\tilde{h}_E+\tilde{\delta}) & z > L, \\ \varphi_{E,n+1}^{b}(z)\big|_{\mathrm{c}} & 0 \leqslant z \leqslant L, \\ d_{E,n+1}^{b}\,\mathrm{D}(\tilde{z}-\tilde{h}_E+\tilde{\delta}) & z < 0, \end{cases} \quad (33)$$

and

$$\varphi_{E,n}^{a}(z)\big|_{\mathrm{c}} = \cos\theta_n\Big(A_n^{+}\,\mathrm{Ai}(\tilde{z}-\tilde{h}_E+\tilde{h}_n^{+}) + B_n^{+}\,\mathrm{Bi}(\tilde{z}-\tilde{h}_E+\tilde{h}_n^{+})\Big) - \sin\theta_n\Big(A_n^{-}\,\mathrm{Ai}(\tilde{z}-\tilde{h}_E+\tilde{h}_n^{-}) + B_n^{-}\,\mathrm{Bi}(\tilde{z}-\tilde{h}_E+\tilde{h}_n^{-})\Big), \quad (34a)$$

$$\varphi_{E,n+1}^{b}(z)\big|_{\mathrm{c}} = \sin\theta_n\Big(A_n^{+}\,\mathrm{Ai}(\tilde{z}-\tilde{h}_E+\tilde{h}_n^{+}) + B_n^{+}\,\mathrm{Bi}(\tilde{z}-\tilde{h}_E+\tilde{h}_n^{+})\Big) + \cos\theta_n\Big(A_n^{-}\,\mathrm{Ai}(\tilde{z}-\tilde{h}_E+\tilde{h}_n^{-}) + B_n^{-}\,\mathrm{Bi}(\tilde{z}-\tilde{h}_E+\tilde{h}_n^{-})\Big). \quad (34b)$$

The coefficients $a_{E,n}^{a}$, $a_{E,n+1}^{b}$, $d_{E,n}^{a}$, $d_{E,n+1}^{b}$, A_n^{+}, A_n^{-}, B_n^{+}, and B_n^{-} in expressions (32–34) are found by imposing the continuity conditions on the wave function and its first derivative at the cavity interfaces.

3 Induced emission probability

In this section, we derive a formula for the induced emission probability of a photon inside the cavity. To this end, we will use simple physical arguments rather than a rigorous treatment based on wavepackets like in reference [29] as these two approaches give the same result. According to equations (32–33) a monoenergetic excited atom coming upwards with unit amplitude upon the cavity that contains n photons is found to move back downwards below the cavity in the $|a\rangle$ state with amplitude $d_{E,n}^{a}$ and similarly in the $|b\rangle$ state with amplitude $d_{E,n+1}^{b}$. As the probability current density of the downward wave does not depend on the energy (see Eq. (21)), the induced emission

probability $\mathcal{P}_{\rm em}(n)$ of a photon inside the cavity containing initially n photons is simply given by

$$\mathcal{P}_{\rm em}(n) = \left|d^b_{E,n+1}\right|^2, \tag{35}$$

and one has

$$\left|d^b_{E,n+1}\right|^2 + \left|d^a_{E,n}\right|^2 = 1. \tag{36}$$

As shown in Appendix A, this probability can be expressed as a function of the sole wave function component $\varphi^a_{E,n}$ of the excited atom inside the cavity through the relation

$$\mathcal{P}_{\rm em}(n) = \pi^2 \tilde{h}^2_{\rm int} \left| \int_{-\infty}^{+\infty} u(\tilde{z})\, \varphi^a_{E,n}(\tilde{z})\, {\rm Ai}\big(\tilde{z} - \tilde{h}_E + \tilde{\delta}\big)\, {\rm d}\tilde{z} \right|^2, \tag{37}$$

valid for any mode function $u(z)$. This relation will help us giving a physical interpretation to our results.

Another relation involving the induced emission probability follows from a certain symmetry of Hamiltonian (1). Denoting the induced emission probability for a total energy E and a detuning δ by $\mathcal{P}_{\rm em}(\tilde{h}_E, \tilde{\delta})$, it can be easily proven that for any mode function $u(z)$ we have

$$\mathcal{P}_{\rm em}(\tilde{h}_E, -\tilde{\delta}) = \mathcal{P}_{\rm em}(\tilde{h}_E + \tilde{\delta}, \tilde{\delta}). \tag{38}$$

We study hereafter the properties of the induced emission probability $\mathcal{P}_{\rm em}(n)$ depending on whether the atomic kinetic energy (or the lack of this energy) at the cavity interfaces is much higher than the interaction energy ($|h_E| \gg h_{\rm int}$ and $|h_E - L| \gg h_{\rm int}$) or much lower. We call each case the classical and quantum regime, respectively.

3.1 Classical regime: Rabi limit

At resonance ($\omega = \omega_0$), it has been shown in reference [29] that the induced emission probability (35) reduces, in the classical regime ($|h_E| \gg h_{\rm int}$ and $|h_E - L| \gg h_{\rm int}$), to the well-known Rabi formula [32]

$$\mathcal{P}_{\rm em}(n) = \sin^2\left(\frac{\Omega_n \tau}{2}\right), \tag{39}$$

where τ is the classical transit time of an atom of energy E through the cavity, indicating that way that the quantization of the atomic motion is unnecessary in this particular regime. The formula generalizing equation (39) in the presence of a detuning δ can be easily derived using the classical results of the interaction of a two-level atom with a quantized electromagnetic field [32] and is given by

$$\mathcal{P}_{\rm em}(n) = \left(\frac{\Omega_n}{\Omega'_n}\right)^2 \times \begin{cases} 4\sin^2\frac{\Omega'_n\tau_2}{2} \\ \times\Big[\cos\frac{\Omega'_n\tau_2}{2}\cos\frac{\delta T}{2} - \frac{\delta}{\Omega'_n}\sin\frac{\Omega'_n\tau_2}{2}\sin\frac{\delta T}{2}\Big]^2 & L < h_E, \\ \sin^2\frac{\Omega'_n\tau_1}{2} & 0 \leqslant h_E \leqslant L, \\ 0 & h_E < 0, \end{cases} \tag{40}$$

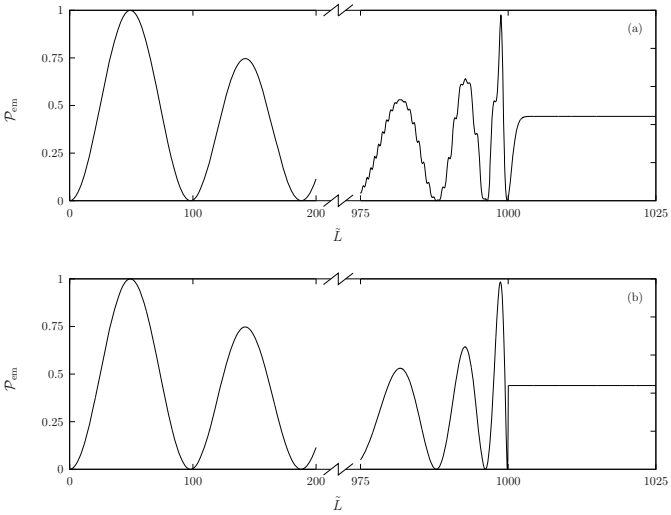

Fig. 3. Induced emission probability $\mathcal{P}_{\rm em}$ with respect to the cavity length (a) with and (b) without quantization of the atomic motion (classical regime: $\tilde{h}_E = 1000$, $\tilde{h}_{\rm int} = 1$ and $\tilde{\delta} = -0.2$).

where τ_1 and τ_2 are the classical interaction times for $0 \leqslant h_E \leqslant L$ and $L < h_E$, respectively. For $\tilde{h}_E < 0$, the atom does not reach the cavity and no induced emission process can occur (the classical interaction time τ is null). For $0 < \tilde{h}_E < \tilde{L}$, the atom turns back inside the cavity and the interaction time τ_1 does not depend on the cavity length L. For $\tilde{h}_E > \tilde{L}$, the atom passes twice inside the cavity (upwards and downwards) and the interaction time τ_2 is L dependent. We will denote the time which passed between the first and the second interaction by T. In terms of dimensionless variables, these various times are given by

$$\Omega'_n\tau_2 = \sqrt{\tilde{\delta}^2 + 4\,\tilde{h}^2_{\rm int}}\left(\sqrt{\tilde{h}_E} - \sqrt{\tilde{h}_E - \tilde{L}}\right), \tag{41}$$

$$\Omega'_n\tau_1 = 2\sqrt{\tilde{\delta}^2 + 4\,\tilde{h}^2_{\rm int}}\,\sqrt{\tilde{h}_E}, \tag{42}$$

$$\delta T = 2\tilde{\delta}\sqrt{\tilde{h}_E - \tilde{L}}. \tag{43}$$

We illustrate in Figures 3a and 3b the induced emission probability $\mathcal{P}_{\rm em} \equiv \mathcal{P}_{\rm em}(n)$ with respect to the cavity length for $\tilde{h}_E \gg \tilde{h}_{\rm int}$, respectively with and without quantization of the atomic motion (Eqs. (35) and (40) respectively). We observe that both results are in good agreement, except in the region where $\tilde{L} \approx \tilde{h}_E$. In this region, $|\tilde{h}_E - \tilde{L}|$ is not much greater than $\tilde{h}_{\rm int}$ and we are out of the validity domain of the approximated expression (40). The small additional oscillations observed in the induced emission probability curve where $\tilde{L} \approx \tilde{h}_E$ are pure quantum effects originating from the quantization of the atomic motion. These effects arise when the cavity length fits nearly the classical turning points of the atoms in the gravitational field. In this case, the potential barrier and well $V^{\pm}_n(z)$ play a significant role as the kinetic energy of the atoms is very small exactly where the potential energy exhibits strong variations.

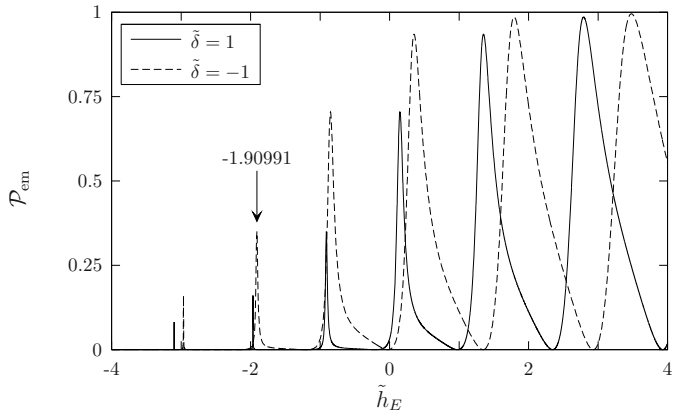

Fig. 4. Induced emission probability with respect to the total atomic energy for $\tilde{L} = 10$, $\tilde{h}_{\rm int} = 10$ and $n = 0$.

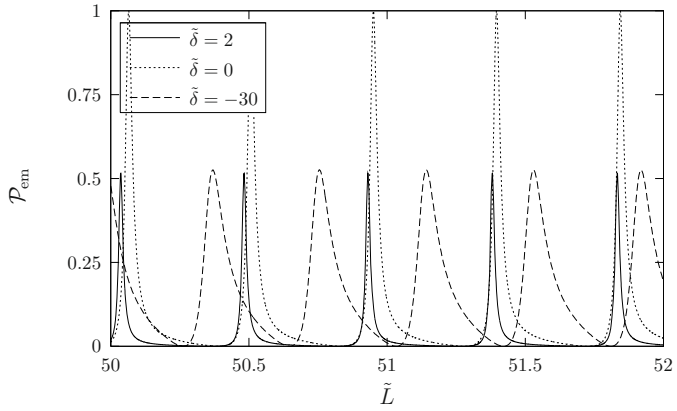

Fig. 5. Induced emission probability with respect to the cavity length for $\tilde{h}_E = 1$, $\tilde{h}_{\rm int} = 100$ and $n = 0$.

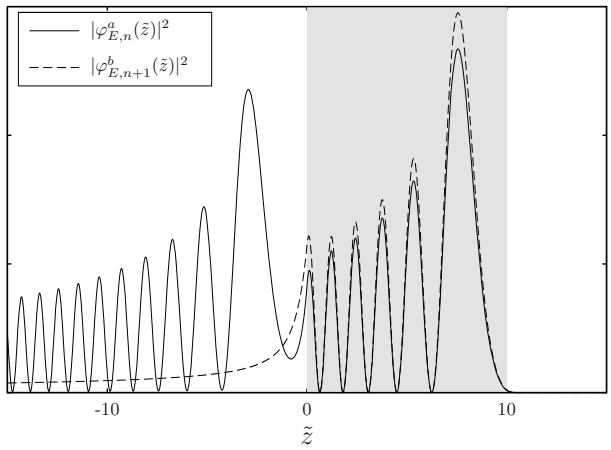

(a) $\tilde{h}_E = -1.90991$ [$\mathcal{P}_{\rm em} \simeq 0.35$]

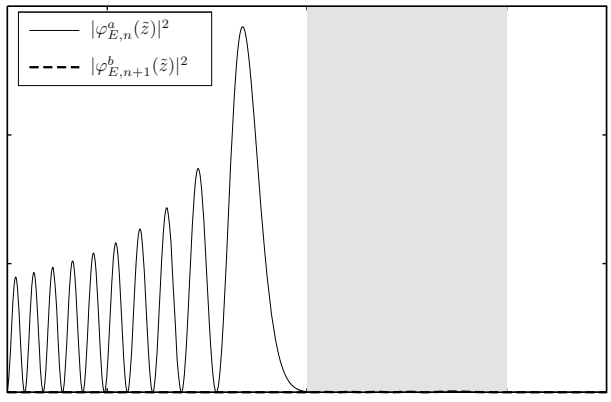

(b) $\tilde{h}_E = -2.2$ [$\mathcal{P}_{\rm em} \simeq 0$]

Fig. 6. Atomic probability densities $|\varphi^a_{E,n}(\tilde{z})|^2$ and $|\varphi^b_{E,n+1}(\tilde{z})|^2$ for $\tilde{L} = 10$, $\tilde{h}_{\rm int} = 10$, $\tilde{\delta} = -1$, and $n = 0$. The grey area shows the cavity region.

3.2 Quantum regime: mazer limit

In the quantum regime, the induced emission probability $\mathcal{P}_{\rm em}$ exhibits a completely different behavior. This is first illustrated in Figures 4 and 5 that show $\mathcal{P}_{\rm em}$ as a function of the total atomic energy and the cavity length, respectively, for nonvanishing detunings. Contrary to the classical regime, narrow resonances are presently observed, even in the negative energy domain ($E < 0$, i.e., $h_E < 0$, see Eq. (2)) where classically the atom does not reach the cavity and cannot therefore emit any photon in there. The existence of negative energy resonances reflects the fact that the atom can still interact with the cavity field for $h_E < 0$ because of the *tunnel effect*. Indeed, we have shown in [29] that at resonance ($\delta = 0$) the total potential felt by the atom in interaction with the cavity possesses quasibound states of negative energy. Whenever such a state energy matches the atomic E value, the atom can enter the cavity by tunnel effect and emit a photon in there. In the presence of a detuning, the emission probability resonances still exist but with a modified position, amplitude, and width.

From a physical point of view, the behavior of the stationary wave functions $\varphi^a_{E,n}(\tilde{z})$ and $\varphi^b_{E,n+1}(\tilde{z})$ (Eqs. (32) and (33)) differs strongly depending on whether the value of the total atomic energy E gives rise or not to a resonance in the emission probability curve (see Fig. 4). This is illustrated in Figures 6a and 6b that show the atomic probability densities $|\varphi^a_{E,n}(\tilde{z})|^2$ and $|\varphi^b_{E,n+1}(\tilde{z})|^2$ inside and outside the cavity (grey and white area respectively). In the first case, the atom is launched upwards to the cavity with a total energy $\tilde{h}_E = -1.90991$ matching a resonance in the emission probability curve (see Fig. 4) and the stationary wave functions $\varphi^a_{E,n}(\tilde{z})$ and $\varphi^b_{E,n+1}(\tilde{z})$ take a significant value inside the cavity. Consequently, a strong interaction between the atom and the cavity field can occur and the induced emission probability is significant, according to equation (37). When considering a realistic atomic wave packet, this effect is of course restricted to the components of the wave packet for which $\tilde{h}_E$ falls within the width of the resonance. Inversely, if the total atomic energy does not match a resonance energy (Fig. 6b), the stationary wave functions are almost zero inside the cavity and no atom-field interaction can take place. In this

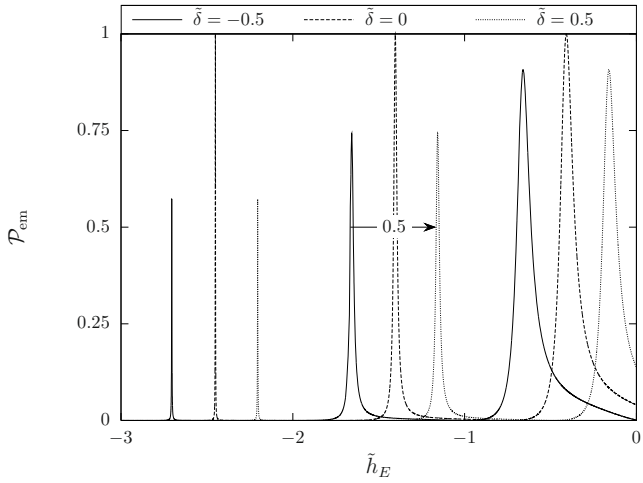

Fig. 7. Induced emission probability with respect to $\tilde{h}_E$ for $\tilde{h}_{\rm int} = 10$, $n = 0$, and $\tilde{L} \gg \tilde{h}_E + \tilde{h}_{\rm int}$.

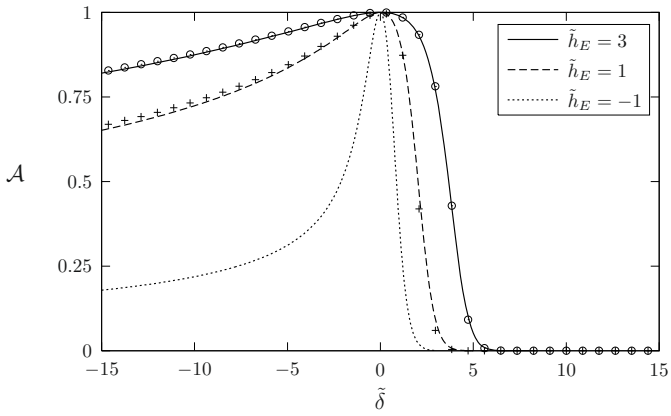

Fig. 8. Amplitude $\mathcal{A}$ of the resonances in the induced emission probability with respect to $\tilde{\delta}$ for $\tilde{h}_{\rm int} = 100$ and $n = 0$. Circles and crosses are the values computed from (46) for $\tilde{h}_E = 3$ and $\tilde{h}_E = 1$ respectively.

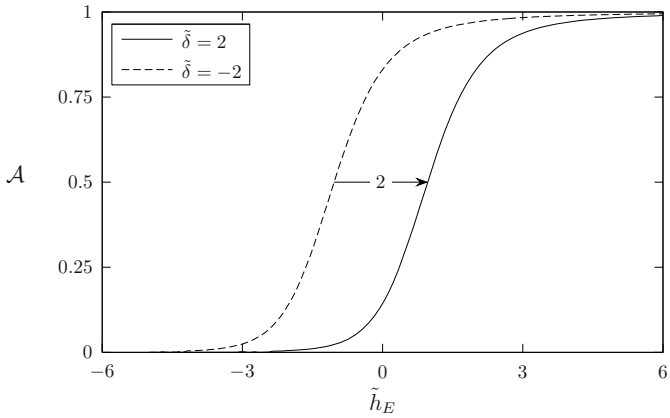

Fig. 9. Amplitude $\mathcal{A}$ of the resonances in the induced emission probability with respect to $\tilde{h}_E$ for $\tilde{h}_{\rm int} = 100$ and $n = 0$.

case, the induced emission probability drops down to zero according to equation (37).

3.2.1 Peak position

Figure 7 shows the induced emission probability for a positive, a negative and a null detuning. We observe that for positive detunings, the emission probability peaks move towards increasing energies while for negative ones it is the opposite. According to equation (38), peaks for opposite detunings $\pm\tilde{\delta}$ are separated in energy by $\tilde{\delta}$ (0.5 in the case of Fig. 7). From Figure 7 and further calculations, it turns out that the peak energy shift caused by a detuning $\pm\delta$ is in very good approximation given by $\pm\tilde{\delta}/2$.

3.2.2 Peak amplitude and width

Figure 8 shows how the peak amplitude evolves with respect to the detuning for various fixed values of the total atomic energy. In contrast to the classical regime (see Eq. (40)), the curves present a strong asymmetry with respect to the sign of the detuning. This results from the atomic energy variation $\hbar\delta$ when the atom emits a photon inside the cavity (see Sect. 2.2). The smaller the total atomic energy is, the more pronounced this asymmetry is. The induced emission probability tends very rapidly to zero for positive detunings, in contrast to what happens for negative detunings. This behavior is already present in equation (37) where the Airy Ai function decreases much faster for large positive arguments than for large negative arguments as can be seen from the asymptotic expansions [30]

$$\mathrm{Ai}(-z) = \frac{z^{-1/4}}{\sqrt{\pi}} \sin\left(\xi + \frac{\pi}{4}\right) + \mathcal{O}\left(z^{-7/4}\right) \qquad (44)$$

$$\mathrm{Ai}(z) = \frac{1}{2\sqrt{\pi}}\, z^{-1/4} e^{-\xi} + \mathcal{O}\left(z^{-7/4} e^{-\xi}\right) \qquad (45)$$

valid for $|z| \gg 1$ and where $\xi = \frac{2}{3} z^{3/2}$.

This asymmetry was also present in the absence of gravity [16] (horizontal geometry, see Fig. 1). In reference [16], it had been shown that the induced emission probability is strictly null for $\hbar\delta > E$. This results merely from energy conservation. If the initial atomic kinetic energy E is lower than $\hbar\delta$, the transition $|a, n\rangle \to |b, n+1\rangle$ cannot take place (as it would remove $\hbar\delta$ from the kinetic energy) and no photon can be emitted inside the cavity. In this case the emission process is completely blocked. In the presence of gravity, there doesn't exist such a threshold. For instance, we can see in Figure 8 that the peak amplitude for $\tilde{h}_E = 3$ takes significant values beyond $\tilde{h}_\delta = 3$. This is not really surprising since quantum mechanically a particle of energy E moving freely in the gravity field is described by the wave function $\varphi(\tilde{z}) = N\mathrm{Ai}(\tilde{z} - \tilde{h}_E)$ and has a nonvanishing probability of being found in the nonclassical region $z > h_E$. This probability decreases however very fast as a function of the height z. This enables us to understand qualitatively why the peak amplitude decreases very rapidly but not sharply (no threshold as

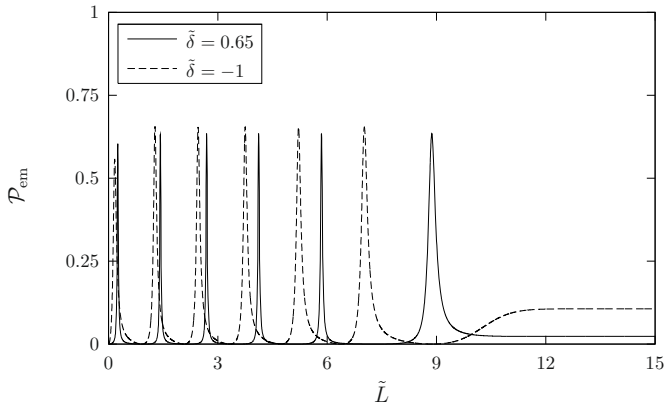

Fig. 10. Induced emission probability with respect to the cavity length for $\tilde{h}_E = -1$, $\tilde{h}_{\rm int} = 10$ and $n = 0$.

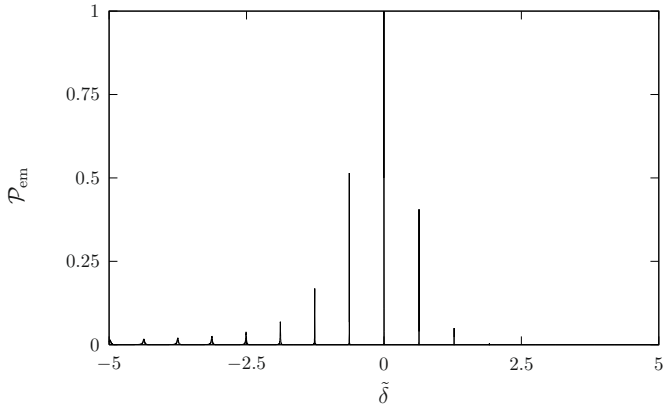

Fig. 11. Induced emission probability with respect to the detuning for $\tilde{h}_E = -2.5$, $\tilde{h}_{\rm int} = 100$, $n = 0$, and $\tilde{L} \gg \tilde{h}_E + \tilde{h}_{\rm int}$. For rubidium atoms, the central peak has a width of only 0.3 Hz.

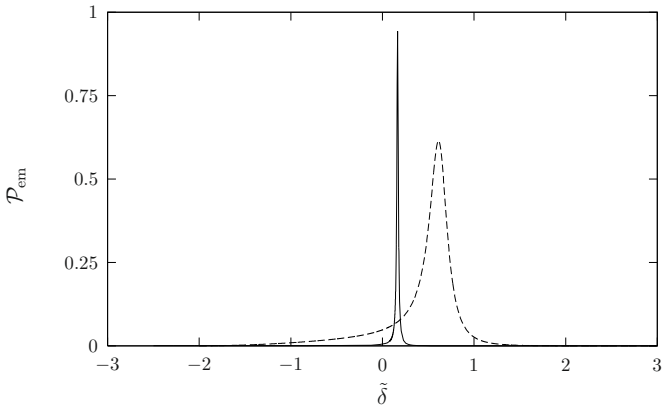

Fig. 12. Induced emission probability with respect to the detuning for a sine mode with $\tilde{h}_{\rm int} = 100$, $\tilde{L} = 10$ (solid line) and for a Gaussian mode with $\tilde{h}_{\rm int} = 10$, $\tilde{L} = 1$ (dashed line) ($\tilde{h}_E = -2$ and $n = 0$ in both cases).

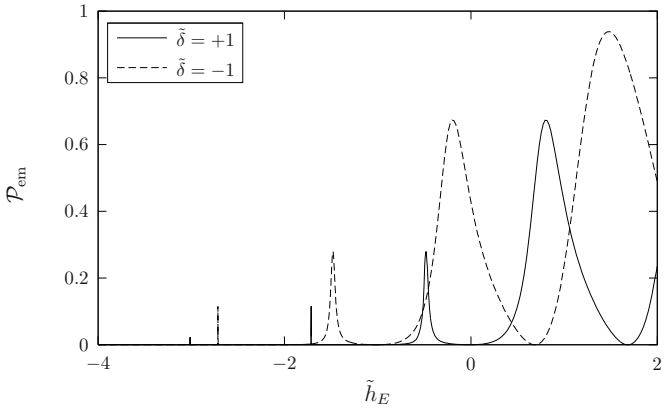

Fig. 13. Induced emission probability with respect to the total atomic energy for a sine mode and $\tilde{h}_{\rm int} = 10$, $\tilde{L} = 10$ and $n = 0$.

in the case of the horizontal mazer) as a function of the detuning for $\tilde{\delta} > \tilde{h}_E$.

Figure 9 shows the peak amplitude with respect to the total atomic energy for two opposite values of the detuning $\tilde{\delta} = \pm 2$. According to equation (38), the curves have the same shape and are merely shifted in energy by $\tilde{h}_E = 2$.

We have observed that the peak amplitude only slightly depends on the interaction height $\tilde{h}_{\rm int}$ and that it is well approximated by the following simple analytical formula

$$\mathcal{A} = \frac{4}{\pi^2}\left|\mathrm{U}(-\tilde{h}_E)\mathrm{D}'(\tilde{\delta}-\tilde{h}_E) - \mathrm{D}(\tilde{\delta}-\tilde{h}_E)\mathrm{U}'(-\tilde{h}_E)\right|^{-2} \quad (46)$$

In Figure 8, we compare the peak amplitude derived from equation (35) and computed from equation (46), respectively. For $\tilde{h}_E = 3$ and higher values of the energy, a good agreement is observed. However, this agreement lowers as the energy decreases.

Concerning the peak width, we have observed that negative detunings increase the peak width while positive ones decrease it (see for example Fig. 5).

3.2.3 Cavity length effects

In the classical regime and in the positive energy domain, the induced emission probability does not depend on the cavity length L as soon as this length is greater than h_E (see Eq. (40)). In the quantum regime, this statement must be revised and holds only when $L \gtrsim h_E + h_n^+$. This is illustrated in Figure 10 which shows the induced emission probability $\mathcal{P}_{\rm em}$ with respect to the cavity length for $\tilde{h}_E = -1$ and $\tilde{h}_{\rm int} = 10$. For $\tilde{h}_\delta = -1$, $\mathcal{P}_{\rm em}$ starts to be constant only beyond $\tilde{L} = \tilde{h}_E + \tilde{h}_n^+ \simeq 8.512$.

3.2.4 Detuning sensitiveness

Figure 11 displays the induced emission probability with respect to the detuning. For realistic experimental parameters [11] and rubidium atoms, these resonances may even become extremely narrow. Their width amounts only 0.3 Hz for $\tilde{h}_E = -2.5$ and $\tilde{h}_{\rm int} = 100$. This could define very useful metrology devices (atomic clocks for example) based on a single cavity and with better performances than what is usually obtained in the well-known Ramsey configuration [33].

3.3 Sine and Gaussian mode functions

The narrow resonances of the induced emission probability observed in the quantum regime are not restricted to the case of the mesa mode investigated so far here. Using numerical procedures (see Appendix B), we have computed the solutions $\varphi^a_{E,n}(\tilde{z})$ and $\varphi^b_{E,n+1}(\tilde{z})$ of the stationary Schrödinger equation (14) for sine and Gaussian mode functions ($u(z) = \sin(\pi z/L)$ for $0 < z < L$, 0 elsewhere and $u(z) = e^{-(z-L/2)^2/2\sigma^2}$ with $\sigma = L/\sqrt{2}$, respectively). We show in Figure 12 the related induced emission probability $\mathcal{P}_{\rm em}$ with respect to the detuning. Again, we observe sharp resonances whose width decreases with increasing interaction height ($h_{\rm int}$).

As any mode function will give rise to such resonances (provided $\tilde{h}_{\rm int}$ is large enough), the resonances in the induced emission probability will be a very general feature of the vertical micromaser in the cold atom regime, in contrast to what happens with the horizontal micromaser where the induced emission probability characteristics are much more mode dependent [11]. This defines a very interesting property as it should help the experimenters to observe the particular behavior of the induced emission probability in the quantum regime, whatever the exact mode function of the cavity. Another nice illustration of the symmetry relation (38) is displayed in Figure 13, this time for a sine mode function.

4 Summary

In this paper we have presented the quantum theory of the vertical mazer for a non resonant atom-field interaction. We have obtained analytical expressions for the wave function in the special case of a constant cavity mode function. The properties of the induced emission probability in the presence of a detuning have been discussed both in the classical and the quantum regimes. The classical results are well recovered for hot atoms for which the quantization of the atomic motion is unnecessary. We have shown that atoms which classically would not reach the interaction region are able to emit a photon inside the cavity. In the quantum regime, the mazer properties are not symmetric with respect to the sign of the detuning and the system exhibits a sharp response as a function of the detuning. The induced emission probability has also been computed for sine and Gaussian mode functions (see Appendix B for the numerical procedure we have developed).

This work has been supported by the Belgian Institut Interuniversitaire des Sciences Nucléaires (IISN). J. Martin thanks the Belgian FRIA for financial support and the University of Liège where part of this work has been done. J. Martin also thanks the French ANR (project INFOSYSQQ, contract number ANR-05-JCJC-0072) for funding.

Appendix A

In this appendix, we derive equation (37) which expresses the induced emission probability as a function of the stationary wave function of the excited atom inside the cavity. To this end, let us recall the equations of motion (14) for the wave function components $\varphi^a_{E,n}$ and $\varphi^b_{E,n+1}$ (see Eq. (10))

$$\left(\frac{\mathrm{d}^2}{\mathrm{d}\tilde{z}^2} - \tilde{z} + \tilde{h}_E\right)\varphi^a_{E,n}(\tilde{z}) = \tilde{h}_{\rm int}\, u(\tilde{z})\, \varphi^b_{E,n+1}(\tilde{z}), \quad \text{(A.1a)}$$

$$\left(\frac{\mathrm{d}^2}{\mathrm{d}\tilde{z}^2} - \tilde{z} + \tilde{h}_E - \tilde{\delta}\right)\varphi^b_{E,n+1}(\tilde{z}) = \tilde{h}_{\rm int}\, u(\tilde{z})\, \varphi^a_{E,n}(\tilde{z}). \quad \text{(A.1b)}$$

To solve the problem numerically, the domain is restricted to $[\tilde{z}_{\rm min}, \tilde{z}_{\rm max}]$. Outside this domain, the mode function $u(\tilde{z})$ is regarded as null.

The outgoing Green function of the stationary Schrödinger equation of a particle of energy E in the gravitational field, satisfying

$$\left(\frac{\mathrm{d}^2}{\mathrm{d}\tilde{z}^2} - \tilde{z} + \tilde{h}_E\right) G_E(\tilde{z}|\tilde{z}') = \delta(\tilde{z} - \tilde{z}'), \quad \text{(A.2)}$$

is given by [34]

$$G_E(\tilde{z}|\tilde{z}') = -i\pi\, \mathrm{D}(\alpha_{E,-})\, \mathrm{Ai}(\alpha_{E,+}) \quad \text{(A.3)}$$

with

$$\alpha_{E,\pm} = -\tilde{h}_E + \frac{(\tilde{z} + \tilde{z}') \pm |\tilde{z} - \tilde{z}'|}{2}. \quad \text{(A.4)}$$

On the one hand, considering the right-hand side term of equation (A.1b) as a source term and using Green function (A.3), the wave function component $\varphi^b_{E,n+1}(\tilde{z})$ is given at $\tilde{z} = \tilde{z}_{\rm min}$ by

$$\varphi^b_{E,n+1}(\tilde{z}_{\rm min}) = -i\pi\tilde{h}_{\rm int}\, \mathrm{D}\big(\tilde{z}_{\rm min} - \tilde{h}_E + \tilde{\delta}\big) \times \int_{-\infty}^{+\infty} u(\tilde{z})\, \varphi^a_{E,n}(\tilde{z})\, \mathrm{Ai}\big(\tilde{z} - \tilde{h}_E + \tilde{\delta}\big)\, \mathrm{d}\tilde{z} \quad \text{(A.5)}$$

since by definition $u(\tilde{z}) = 0$ for $\tilde{z} < \tilde{z}_{\rm min}$. On the other hand, $\varphi^b_{E,n+1}(\tilde{z})$, which is continuous at $\tilde{z} = \tilde{z}_{\rm min}$, is also given by equation (19). Identification with equation (A.5) then yields

$$d^b_{E,n+1} = -i\pi\tilde{h}_{\rm int} \int_{-\infty}^{+\infty} u(\tilde{z})\, \varphi^a_{E,n}(\tilde{z})\, \mathrm{Ai}\big(\tilde{z} - \tilde{h}_E + \tilde{\delta}\big)\, \mathrm{d}\tilde{z} \quad \text{(A.6)}$$

whose absolute value squared gives equation (37).

Appendix B

In this appendix, we describe the method we have developed to solve numerically the system (A.1) of coupled differential equations with imposed boundary conditions.

B.1 Boundary conditions

The continuity conditions of the wave function components (18) and (19) and their first derivatives at the cavity interfaces ($\tilde{z}_{\min}$ and $\tilde{z}_{\max}$) read

$$\begin{cases} \varphi^a_{E,n}(\tilde{z}_{\min}) &= \mathrm{U}\big(\tilde{z}_{\min}-\tilde{h}_E\big)+d^a_{E,n}\,\mathrm{D}\big(\tilde{z}_{\min}-\tilde{h}_E\big) \\ \frac{\mathrm{d}\varphi^a_{E,n}}{\mathrm{d}\tilde{z}}(\tilde{z}_{\min}) &= \mathrm{U}'\big(\tilde{z}_{\min}-\tilde{h}_E\big)+d^a_{E,n}\,\mathrm{D}'\big(\tilde{z}_{\min}-\tilde{h}_E\big) \\ \varphi^b_{E,n+1}(\tilde{z}_{\min}) &= d^b_{E,n+1}\,\mathrm{D}\big(\tilde{z}_{\min}+\tilde{\delta}-\tilde{h}_E\big) \\ \frac{\mathrm{d}\varphi^b_{E,n+1}}{\mathrm{d}\tilde{z}}(\tilde{z}_{\min}) &= d^b_{E,n+1}\,\mathrm{D}'\big(\tilde{z}_{\min}+\tilde{\delta}-\tilde{h}_E\big) \end{cases} \tag{B.1}$$

and

$$\begin{cases} \varphi^a_{E,n}(\tilde{z}_{\max}) &= a^a_{E,n}\,\mathrm{Ai}\big(\tilde{z}_{\max}-\tilde{h}_E\big) \\ \frac{\mathrm{d}\varphi^a_{E,n}}{\mathrm{d}\tilde{z}}(\tilde{z}_{\max}) &= a^a_{E,n}\,\mathrm{Ai}'\big(\tilde{z}_{\max}-\tilde{h}_E\big) \\ \varphi^b_{E,n+1}(\tilde{z}_{\max}) &= a^b_{E,n+1}\,\mathrm{Ai}\big(\tilde{z}_{\max}+\tilde{\delta}-\tilde{h}_E\big) \\ \frac{\mathrm{d}\varphi^b_{E,n+1}}{\mathrm{d}\tilde{z}}(\tilde{z}_{\max}) &= a^b_{E,n+1}\,\mathrm{Ai}'\big(\tilde{z}_{\max}+\tilde{\delta}-\tilde{h}_E\big) \end{cases} \tag{B.2}$$

From equation (B.2), we can construct the following boundary conditions (BC)

$$\begin{cases} \varphi^a_{E,n}(\tilde{z}_{\max}) &= a^a_{E,n}\,\mathrm{Ai}\big(\tilde{z}_{\max}-\tilde{h}_E\big) \\ \frac{\mathrm{d}\varphi^a_{E,n}}{\mathrm{d}\tilde{z}}(\tilde{z}_{\max}) &= a^a_{E,n}\,\mathrm{Ai}'\big(\tilde{z}_{\max}-\tilde{h}_E\big) \\ \frac{\mathrm{d}\varphi^b_{E,n+1}}{\mathrm{d}\tilde{z}}(\tilde{z}_{\max}) &= \frac{\mathrm{Ai}'\big(\tilde{z}_{\max}+\tilde{\delta}-\tilde{h}_E\big)}{\mathrm{Ai}\big(\tilde{z}_{\max}+\tilde{\delta}-\tilde{h}_E\big)}\,\varphi^b_{E,n+1}(\tilde{z}_{\max}) \end{cases} \tag{B.3}$$

B.2 Resolution scheme

We first introduce the vector $\overrightarrow{\varphi}(\tilde{z}) = \big(\varphi^a_{E,n}(\tilde{z}),\varphi^b_{E,n+1}(\tilde{z})\big)^{\mathrm{T}}$. Now, let $\overrightarrow{\varphi}_1(\tilde{z})$ and $\overrightarrow{\varphi}_2(\tilde{z})$ be two vectors satisfying (14) with the boundary conditions (at $\tilde{z}=\tilde{z}_{\max}$)

$$(1)\begin{cases} \varphi^a_{E,n}(\tilde{z}_{\max}) &= \mathrm{Ai}\big(\tilde{z}_{\max}-\tilde{h}_E\big) \\ \frac{\mathrm{d}\varphi^a_{E,n}}{\mathrm{d}\tilde{z}}(\tilde{z}_{\max}) &= \mathrm{Ai}'\big(\tilde{z}_{\max}-\tilde{h}_E\big) \\ \varphi^b_{E,n+1}(\tilde{z}_{\max}) &= 0 \\ \frac{\mathrm{d}\varphi^b_{E,n+1}}{\mathrm{d}\tilde{z}}(\tilde{z}_{\max}) &= 0 \end{cases} \tag{B.4}$$

and

$$(2)\begin{cases} \varphi^a_{E,n}(\tilde{z}_{\max}) &= \mathrm{Ai}\big(\tilde{z}_{\max}-\tilde{h}_E\big) \\ \frac{\mathrm{d}\varphi^a_{E,n}}{\mathrm{d}\tilde{z}}(\tilde{z}_{\max}) &= \mathrm{Ai}'\big(\tilde{z}_{\max}-\tilde{h}_E\big) \\ \varphi^b_{E,n+1}(\tilde{z}_{\max}) &= 1 \\ \frac{\mathrm{d}\varphi^b_{E,n+1}}{\mathrm{d}\tilde{z}}(\tilde{z}_{\max}) &= \frac{\mathrm{Ai}'\big(\tilde{z}_{\max}+\tilde{\delta}-\tilde{h}_E\big)}{\mathrm{Ai}\big(\tilde{z}_{\max}+\tilde{\delta}-\tilde{h}_E\big)}. \end{cases} \tag{B.5}$$

The most general solution consistent with BC (B.3) is then given by

$$\overrightarrow{\varphi}_{\mathrm{right}}(\tilde{z}) = \alpha\,\overrightarrow{\varphi}_1(\tilde{z}) + (a^a_{E,n}-\alpha)\,\overrightarrow{\varphi}_2(\tilde{z}) \tag{B.6}$$

where α and $a^a_{E,n}$ are constants.

Next, let $\overrightarrow{\varphi}_3(\tilde{z})$, $\overrightarrow{\varphi}_4(\tilde{z})$ and $\overrightarrow{\varphi}_5(\tilde{z})$ be three vectors satisfying (14) with the boundary conditions (at $\tilde{z}=\tilde{z}_{\min}$)

$$(3)\begin{cases} \varphi^a_{E,n}(\tilde{z}_{\min}) &= \mathrm{U}\big(\tilde{z}_{\min}-\tilde{h}_E\big) \\ \frac{\mathrm{d}\varphi^a_{E,n}}{\mathrm{d}\tilde{z}}(\tilde{z}_{\min}) &= \mathrm{U}'\big(\tilde{z}_{\min}-\tilde{h}_E\big) \\ \varphi^b_{E,n+1}(\tilde{z}_{\min}) &= 0 \\ \frac{\mathrm{d}\varphi^b_{E,n+1}}{\mathrm{d}\tilde{z}}(\tilde{z}_{\min}) &= 0, \end{cases} \tag{B.7}$$

$$(4)\begin{cases} \varphi^a_{E,n}(\tilde{z}_{\min}) &= \mathrm{D}\big(\tilde{z}_{\min}-\tilde{h}_E\big) \\ \frac{\mathrm{d}\varphi^a_{E,n}}{\mathrm{d}\tilde{z}}(\tilde{z}_{\min}) &= \mathrm{D}'\big(\tilde{z}_{\min}-\tilde{h}_E\big) \\ \varphi^b_{E,n+1}(\tilde{z}_{\min}) &= 0 \\ \frac{\mathrm{d}\varphi^b_{E,n+1}}{\mathrm{d}\tilde{z}}(\tilde{z}_{\min}) &= 0, \end{cases} \tag{B.8}$$

and

$$(5)\begin{cases} \varphi^a_{E,n}(\tilde{z}_{\min}) &= 0 \\ \frac{\mathrm{d}\varphi^a_{E,n}}{\mathrm{d}\tilde{z}}(\tilde{z}_{\min}) &= 0 \\ \varphi^b_{E,n+1}(\tilde{z}_{\min}) &= \mathrm{D}\big(\tilde{z}_{\min}+\tilde{\delta}-\tilde{h}_E\big) \\ \frac{\mathrm{d}\varphi^b_{E,n+1}}{\mathrm{d}\tilde{z}}(\tilde{z}_{\min}) &= \mathrm{D}'\big(\tilde{z}_{\min}+\tilde{\delta}-\tilde{h}_E\big). \end{cases} \tag{B.9}$$

The most general solution consistent with BC (B.1) is then given by

$$\overrightarrow{\varphi}_{\mathrm{left}}(\tilde{z}) = \overrightarrow{\varphi}_3(\tilde{z}) + d^a_{E,n}\,\overrightarrow{\varphi}_4(\tilde{z}) + d^b_{E,n+1}\,\overrightarrow{\varphi}_5(\tilde{z}). \tag{B.10}$$

where $d^a_{E,n}$ et $d^b_{E,n+1}$ are constants.

In order to determine the value of the constants α, $a^a_{E,n}$, $d^a_{E,n}$ and $d^b_{E,n+1}$ appearing in (B.6) and (B.10), we have to solve the system of equations formed by the continuity conditions of the wave function and its first derivative at an intermediate point $\tilde{z}_0 \in [\tilde{z}_{\min},\tilde{z}_{\max}]$

$$\begin{cases} \overrightarrow{\varphi}_{\mathrm{left}}(\tilde{z}_0) &= \overrightarrow{\varphi}_{\mathrm{right}}(\tilde{z}_0) \\ \overrightarrow{\varphi}'_{\mathrm{left}}(\tilde{z}_0) &= \overrightarrow{\varphi}'_{\mathrm{right}}(\tilde{z}_0). \end{cases} \tag{B.11}$$

Once this system has been solved, the value of the amplitude $d^b_{E,n+1}$ is known and the induced emission probability can be computed by use of equation (35).

References

1. C. Cohen-Tannoudji, Phys. Scr. T **76**, 33 (1998)
2. Y. Miroshnychenko, W. Alt, I. Dotsenko, L. Förster, M. Khudaverdyan, D. Meschede, D. Schrader, A. Rauschenbeutel, Nature **442**, 151 (2006)
3. H.A. Klein, G.P. Barwood, P. Gill, G. Huang, Phys. Scr. T **86**, 33 (2000)
4. E.W. Hagley, L. Deng, M. Kozuma, J. Wen, K. Helmerson, S.L. Rolston, W.D. Phillips, Science **283**, 1706 (1999)
5. A. Ruschhaupt, J.G. Muga, Phys. Rev. A **70**, 061604 (2004)
6. A. Ruschhaupt, J.G. Muga, M.G. Raizen, J. Phys. B: At. Mol. Opt. Phys. **39**, (2006)

7. B.T. Seaman, M. Kramer, D.Z. Anderson, M.J. Holland, Phys. Rev. A **75**, 023615 (2007)
8. J.J. García-Ripoll, P. Zoller, J.I. Cirac, J. Phys. B: At. Mol. Opt. Phys. **38**, S567 (2005)
9. M.O. Scully, G.M. Meyer, H. Walther, Phys. Rev. Lett. **76**, 4144 (1996)
10. G.M. Meyer, M.O. Scully, H. Walther, Phys. Rev. A **56**, 4142 (1997)
11. M. Löffler, G.M. Meyer, M. Schröder, M.O. Scully, H. Walther, Phys. Rev. A **56**, 4153 (1997)
12. M. Löffler, G.M. Meyer, H. Walther, Europhys. Lett. **41**, 593 (1998)
13. G.S. Agarwal, R. Arun, Phys. Rev. Lett. **84**, 5098 (2000)
14. R. Arun, G.S. Agarwal, M.O. Scully, H. Walther, Phys. Rev. A **62**, 023809 (2000)
15. R. Arun, G.S. Agarwal, Phys. Rev. A **66**, 043812 (2002)
16. T. Bastin, J. Martin, Phys. Rev. A **67**, 053804 (2003)
17. J. Martin, T. Bastin, Eur. Phys. J. D **29**, 133 (2004)
18. D. Seidel, J.G. Muga, Eur. Phys. J. D **41**, 71 (2007)
19. J. Martin, T. Bastin, Phys. Rev. A **75**, 053820 (2007)
20. H. Walther, B.T.H. Varcoe, B.G. Englert, T. Becker, Rep. Prog. Phys. **69**, 1325 (2006)
21. H. Mabuchi, Q.A. Turchette, M.S. Chapman, J. Kimble, Opt. Lett. **21**, 1393 (1996)
22. C.J. Hood, M.S. Chapman, T.W. Lynn, H.J. Kimble, Phys. Rev. Lett. **80**, 4157 (1998)
23. P. Münstermann, T. Fischer, P. Maunz, P. Pinkse, G. Rempe, Phys. Rev. Lett. **82**, 3791 (1999)
24. P. Münstermann, T. Fischer, P. Pinkse, G. Rempe, Opt. Commun. **159**, 63 (1999)
25. J. Ye, D.W. Vernooy, H.J. Kimble, Phys. Rev. Lett. **24**, 4987 (1999)
26. M. Hennrich, T. Legero, A. Kuhn, G. Rempe, Phys. Rev. Lett. **85**, 4872 (2000)
27. Y. Shimizu, N. Shiokawa, N. Yamamoto, M. Kozuma, T. Kuga, L. Deng, E.W. Hagley, Phys. Rev. Lett. **89**, 233001 (2002)
28. P. Maunz, T. Puppe, I. Schuster, N. Syassen, P.W.H. Pinkse, G. Rempe, Nature **428**, 50 (2004)
29. T. Bastin, J. Martin, Phys. Rev. A **72**, 053815 (2005)
30. M. Abramowitz, I. Stegun, *Handbook of Mathematical Functions* (Dover Publications, New York, 1970)
31. C. Cohen-Tannoudji, J. Dupont-Roc, G. Grynberg, *Processus d'interaction entre photons et atomes* (Savoirs actuels InterEditions/Editions du CNRS, 1988)
32. W.P. Schleich, *Quantum Optics in Phase Space* (WILEY-VCH Verlag Berlin GmbH, Bühringstrasse 10 D-13086 Berlin, 2001)
33. A. Clairon, C. Salomon, S. Guellati, W.D. Phillips, Europhys. Lett. **16**, 165 (1991)
34. C. Bracher, W. Becker, S.A. Gurvitz, M. Kleber, M.S. Marinov, Am. J. Phys. **66**, 38 (1997)